51st AIAA/ASME/ASCE/AHS/ASC Structures, Structural Dynamics, and Materials Conference<BR> 18th
12 - 15 April 2010, Orlando, Florida

AIAA 2010-2964

# Uncertainty Propagation in Hypersonic Aerothermoelastic Analysis

Nicolas Lamorte*, Bryan Glaz† and Peretz P. Friedmann‡
*Department of Aerospace Engineering, The University of Michigan, Ann Arbor, MI, 48109-2140, USA*

Adam J. Culler§, Andrew R. Crowell¶ and Jack J. McNamara‖
*Department of Aerospace Engineering, Ohio State University, Columbus, OH, 43210-1226, USA*

**This study sets the framework for uncertainty propagation in hypersonic aeroelastic and aerothermoelastic stability analyses. First, the aeroelastic stability of typical hypersonic control surface section is considered. Variability in the uncoupled natural frequencies of the system are modeled using beta probability distributions. Uncertainty is propagated to the flutter Mach number using the stochastic collocation approach. In addition, the stability of an aerodynamically heated panel located on a hypersonic vehicle is considered. Uncertainty is identified using CFD tools and it is shown that turbulence modeling has a significant effect on the prediction of the heat flux distribution and transition location. The uncertainties identified are propagated through the system and their effect on the flight of the vehicle is determined. For both cases, uncertainty is treated using stochastic collocation, a relatively new approach that is shown to be very efficient.**

## Nomenclature

| | |
|---|---|
| $a$ | Normalized elastic axis location positive aft from midchord |
| $A, B$ | Coefficients for beta distribution |
| $A_j$ | Fitting coefficients |
| $A_n(t)$ | Deformed shape coefficients |
| $b = c/2$ | Semi chord |
| $c$ | Chord |
| $C_1, C_2, C_3, C_4$ | Deformed shape coefficients |
| $\hat{f}(\xi)$ | Polynomial response surface of the output of interest |
| $h$ | Plunge degree of freedom |
| $H$ | Altitude |
| $h_1$ | Radiation shield thickness |
| $h_2$ | Thermal insulation thickness |
| $h_p$ | Panel thickness |
| $K_\alpha$ | Spring constant in pitch |
| $K_h$ | Spring constant in plunge |
| $l_p$ | Panel length |
| $M$ | Free stream Mach number |
| $M_f$ | Flutter Mach number |
| $M_{f,deter}$ | Deterministic flutter Mach number |

*Ph. D. Candidate, Student Member AIAA.
†Postdoctoral Researcher, Member AIAA.
‡François-Xavier Bagnoud Professor, Fellow AIAA.
§Ph.D. Student, Student Member AIAA.
¶Graduate Research Associate, Student Member AIAA.
‖Assistant Professor, Member AIAA.

| | |
|---|---|
| $N_I$ | Number of points in the numerical integration scheme |
| $N_v$ | Number of random variables |
| $p(\xi)$ | Probability density function (PDF) |
| $P+1$ | Number of interpolating function |
| $p_{(A,B)}(\xi)$ | (A,B) Beta probability density function |
| $Q_{aero}$ | Aerodynamic heat flux |
| $Q_{rad}$ | Radiation heat flux |
| $t$ | Time |
| $t_h/b = \tau$ | Normalized airfoil thickness |
| $T_{wall}$ | Wall temperature |
| $T_f$ | Flight Time |
| $w(x,t)$ | Out of plane panel displacement |
| $w_k$ | Numerical integration scheme weights |
| $x$ | Coordinate on the panel |
| $x_\alpha$ | Normalized center of gravity location positive aft from elastic axis |
| $x_{ti}$ | Location of the transition from laminar to turbulent flow |
| $y = f(\xi)$ | Output of interest |

*Symbols*

| | |
|---|---|
| $\alpha$ | Pitch degree of freedom |
| $\alpha_q$ | Aerodynamic heat flux scaling factor |
| $\beta = \frac{M_f}{M_{f,deter}}$ | Flutter Mach number ratio |
| $\beta_s$ | Shock angle |
| $\delta_{jk}$ | Kronecker symbol |
| $\Gamma$ | Gamma function |
| $\theta$ | Forebody surface inclination |
| $\xi$ | Normalized random variable associated with uncertain input |
| $\boldsymbol{\xi}$ | Vector of uncertain inputs |
| $\xi_k$ | Numerical integration scheme points |
| $\langle\xi\rangle$ | Mean of $\xi$ |
| $\sigma_\xi$ | Standard deviation of $\xi$ |
| $\phi_j(\xi)$ | Interpolating polynomials functions |
| $\omega_\alpha$ | Natural frequency in pitch |
| $\omega_h$ | Natural frequency in plunge |

# I. Introduction

HYPERSONIC flight is an active area of research motivated by interest in unmanned rapid response to threats and reusable launch vehicles for affordable access to space.[1–6] Such vehicles are based on lifting body designs which tightly integrate the airframe and propulsion system. For hypersonic cruise speeds, the propulsion system is based on air-breathing engines that require sustained periods of atmospheric flight.[5,7,8] Flying at hypersonic speeds within the atmosphere causes severe aerodynamic heating effects. Accurate modeling of the resulting aerothermoelastic interactions is critical to hypersonic vehicle performance, stability, and reliability analyses.

Hypersonic flows are inherently complex and involve phenomena that are not present in supersonic conditions; e.g. dissociations, chemically reacting flow, viscous interactions and higher levels of aerodynamic heat flux.[7,8] Similarity laws for aerothermoelastic scaling are not available and therefore the ability to examine the fully coupled aerothermoelastic problem experimentally at reduced scales over the full flight envelop of a hypersonic vehicle is not feasible.[9] Therefore, the development of accurate computational aerothermoelastic simulation capabilities is critical for design and analysis of hypersonic vehicles.

High fidelity numerical simulations of the complex hypersonic flow environment are computationally very expensive and the state of art is still at an early stage of development in which the role of important factors such as real gas effects, chemically reacting flows and complex viscous interactions are not understood. Current analysis tools employ computationally efficient models based on simplifying assumptions of the physics and/or reduced-order modeling of full order computations. Compensating for these shortcomings in

modeling capability, as well as the use of reduced order models (ROM) to enhance computational efficiency, mandates the use of uncertainty propagation techniques in hypersonic aerothermoelastic analyses.

In aerothermoelastic analysis of hypersonic vehicles, two commonly used models based on simplifying assumptions are piston theory for computing the aerodynamic loading,[1] and Eckert's reference temperature or enthalpy method for calculating aerodynamic heat flux.[7] However, the simplifying assumptions, such as the neglect of real gas effects or turbulence modeling, introduce uncertainty associated with the results of the simulation code. In addition, reduced order models (ROM) currently being developed for each component (aerodynamic loading, aerodynamic heating, propulsion, structural dynamics and control) of the hypersonic vehicle[10–15] also introduce error into the analysis. Therefore, for this class of problems, the uncertainty due to both unmodeled physics and the approximation errors associated with ROM's for several components must be propagated through the analysis. Several approaches for propagating uncertainty in aeroelastic problems are available, such as: direct Monte Carlo simulations[16] (MCS), polynomials chaos expansion[17] (PCE), adaptive finite elements.[18] In this study, stochastic collocation (SC) is employed since this method is an effective alternative to direct Monte Carlo simulation, which has prohibitive computational costs for complex problems. Furthermore, SC does not require modifications to deterministic analyses codes (i.e. non-intrusive), and was shown to outperform PCE in a recent study.[19]

The overall objective of this paper is to investigate the effects of several uncertainty sources relevant to hypersonic vehicle design. Stochastic collocation is used to propagate uncertainty associated with two illustrative problems:

1. Aeroelastic stability of a typical section representative of a hypersonic control surface. For this case, the effects of uncertainty associated with the natural bending and torsional frequencies are considered, and SC is used to quantify the effect of uncertainty on the flutter Mach number.

2. Aerothermoelastic stability of a panel located on a vehicle flying at hypersonic speeds. For this case, uncertainties due to modeling assumptions associated with the aerodynamic heat flux and laminar to turbulent transition predictions are quantified, and their effects on flight time before the onset of panel flutter, are studied.

## II. Representative Hypersonic Aeroelastic and Aerothermoelastic studies

Two representative case studies are presented in this section. They represent typical analyses of hypersonic vehicle components. The first study corresponds to the aeroelastic analysis of a typical hypersonic control surface section. Next the aerothermoelastic stability of a panel located on a vehicle flying at hypersonic speed on a straight trajectory is considered. Brief descriptions of the models, as well as the uncertain inputs and outputs of interest associated with each representative study are provided in this section.

### II.A. Aeroelastic Stability of a 2D Typical Section

As an illustrative example of uncertainty effects on the aeroelastic stability characteristics of a hypersonic vehicle, the flutter Mach number associated with a double wedge typical section representative of a control surface is examined. The typical section, shown in Fig. 1, is characterized by pitch ($\alpha$) and plunge ($h$) degrees of freedom. This problem was treated deterministically in Ref. 2.

The output of interest, $y$, is the flutter Mach number which governs system stability. In this study, variability is introduced in the uncoupled natural frequencies, $\omega_\alpha$ and $\omega_h$, to account for uncertainty due to material and mass properties. Therefore, the output of interest for this problem is a function of two uncertain inputs – denoted $\xi_1$ and $\xi_2$ – which correspond to the natural frequencies. The aerodynamic loading is obtained from $3^{rd}$ order piston theory. The aeroelastic stability is determined using an efficient damping identification method known as the ARMA model.[20] Damping is extracted from the transient response of the system. As dynamic pressure increases, flutter ensues and the flutter Mach number $M_f$ corresponds to zero damping in one of the two modes of the system. The flutter Mach number $M_f$ depends also on the offset $a$ between the elastic axis and the mid-chord.

### II.B. Aerothermoelastic Behavior of a Panel

The second problem considered is the aerothermoelastic stability of an aerodynamically heated two-dimensional panel. The panel depicted in Fig. 2(a) is located on the surface of a vehicle flying at hypersonic speeds.

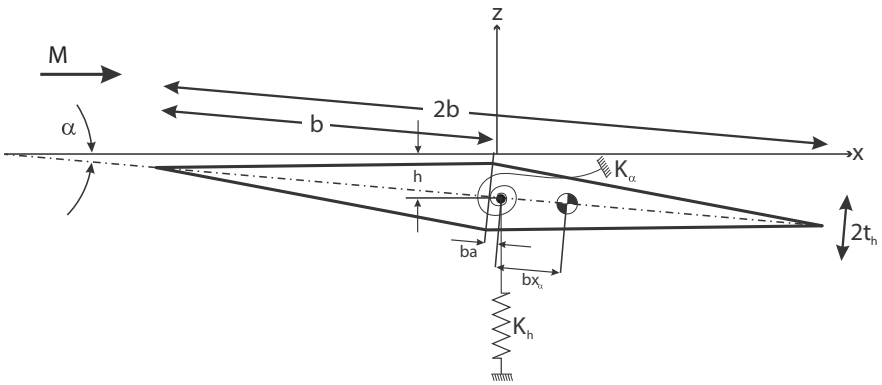


**Figure 1. Two degree-of-freedom typical section geometry**

It is assumed that the panel is covered by a thermal protection system consisting of a radiation shield and thermal insulation, shown in Fig. 2(b).

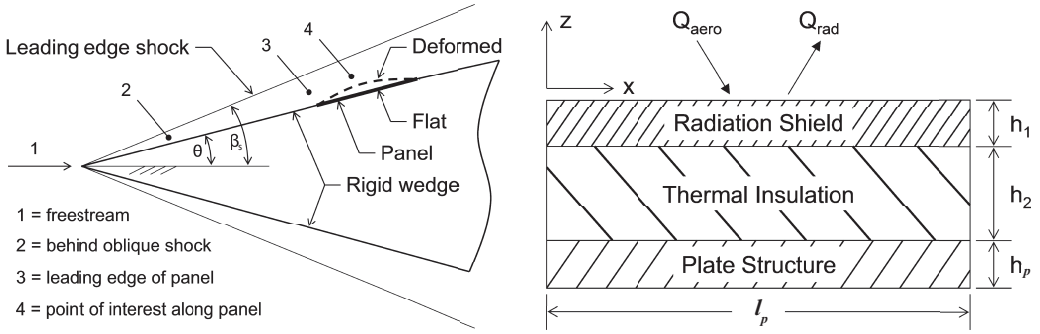


(a) Panel located on an inclined surface of a wedge-shaped forebody

(b) Two-dimensional model of the thermal structure

**Figure 2. Illustration of the panel problem**

A detailed deterministic study of this problem has been performed in Ref. 13. The nonlinear equations of motion are solved using a Galerkin approach to eliminate spatial dependence and the time domain panel response is obtained from a fourth order Runge-Kutta scheme. The out of plane displacement $w(x,t)$, Eq. 1, is expressed as a combination of sine modes and a third order polynomial function uniquely defined to satisfy non–homogeneous boundary conditions due to thermal loads.

$$w(x,t) = \sum_{n=1}^{6} A_n(t) \sin(\frac{n\pi x}{l_p}) + C_1(t) + C_2(t)x + C_3(t)x^2 + C_4(t)x^4 \tag{1}$$

The aeroelastic model for this problem is obtained by combining the two-dimensional, moderate deflection von Karman plate theory with unsteady aerodynamic loading based on $3^{rd}$ order piston theory. The heat transfer problem is treated using Eckert's reference enthalpy model to evaluate the aerodynamic heat flux.[21] The temperature distribution in the structure is computed from a finite difference solution of the heat transfer problem. It is assumed that the vehicle is in straight and level flight, at a constant altitude and Mach number. Since the edges of the panel are fixed at its end points, thermal stresses develop as the panel is heated, causing buckling and eventual aerothermoelastic instability. The instant when the panel starts to flutter determines the flight time, $T_f$, that characterizes the stability boundary of the system. This flight time corresponds to the instant when the out of plane panel displacement at the mid-chord point reaches $-10\%$ of the panel thickness. This value for the out of plane displacement signifies the onset of oscillating values for $w$, which is indicative of panel flutter. This metric for the onset of flutter is accurate to within $\pm 1$ second of flight time.

Since aerodynamic loading, elastic deformation, inertial loads and heat transfer are tightly coupled,[13] heat flux prediction is a key component of the analysis. The use of Eckert's reference enthalpy model implies several assumptions about the modeling of the heating problem which introduce sources of uncertainty and affect the stability of the system. Therefore, uncertainty in the heat flux prediction is quantified. A scaling factor $\alpha_q$ for the heat flux is introduced and treated as the first random variable, $\xi_1$. Transition location, $x_{ti}$, is identified and treated as the second random variable, $\xi_2$.

## III. Uncertainty Propagation

Once the outputs of interest have been defined and the uncertain inputs have been identified, probabilistic approaches can be applied to quantify uncertainty effects. In this study, the effects of uncertain inputs $\xi$ are propagated through a computational analysis symbolically represented by $f$ in order to quantify uncertainty effects on the output of interest $f(\boldsymbol{\xi})$. The uncertainty propagation analysis is illustrated in Fig. 3. The function $f$ represents the aeroelastic or the aerothermoelastic stability analyses described in Section II, where $\boldsymbol{\xi}$ are the uncertain input parameters. The probabilistic approach to uncertainty quantification consists of the following steps:

1. Each uncertain input is treated as a random variable characterized by a probability distribution, $p(\xi)$.
2. Stochastic collocation is used to approximate the computationally expensive functional dependance of the output of interest on the uncertain inputs, i.e. $f(\boldsymbol{\xi})$ is approximated.
3. Conventional MCS methods are applied to the computationally efficient approximate representation obtained from SC. The effects of the uncertain inputs on the output of interest are quantified on terms of probability distributions denoted by $p(y)$.

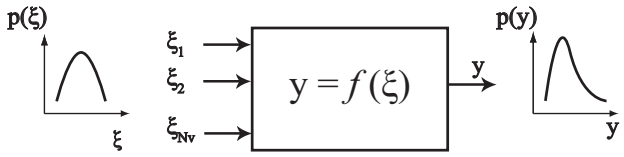


**Figure 3. Uncertainty propagation approach**

Detailed descriptions of the probabilistic characterizations of the uncertain inputs and the SC function approximations are provided in the following subsections.

### III.A. Characterization of Input Probability Distribution

Randomness associated with an uncertain input is modeled by a probability density function (PDF), $p(\xi)$, and $p(\xi_0)d\xi$ is the probability that $\xi_0 - d\xi/2 \leq \xi \leq \xi_0 + d\xi/2$. Thus the PDF $p(\xi_0)$ describes the probability of occurrence that the random variable $\xi$ will have the value of $\xi_0$. Commonly used PDF's include normal, log-normal, exponential or Cauchy distributions which are defined on unbounded domains. Using such PDF's may require evaluating the output of interest at input combinations with no physical significance and/or leading to unfeasible computations. In contrast, beta distributions, given in Eq. 2, represent a family of bounded probability distributions in which the range of the random input variables can be controlled by prescribing bounds. Moreover, the choice of the two parameters $A$ and $B$ permits one to control the PDF shape as illustrated in Fig. 4. Thus, uniform, symmetric or non-symmetric PDF's can be accommodated over the input range by using beta distributions.[22] A beta distribution corresponding to particular values of $A$ and $B$ will be denoted by $Beta(A, B)$.

$$p_{(A,B)}(\xi) = \frac{\Gamma(A+B)}{\Gamma(A)\Gamma(B)} \frac{(1+\xi)^{A-1}(1-\xi)^{B-1}}{2^{A+B-1}}, \quad -1 \leq \xi \leq 1 \tag{2}$$

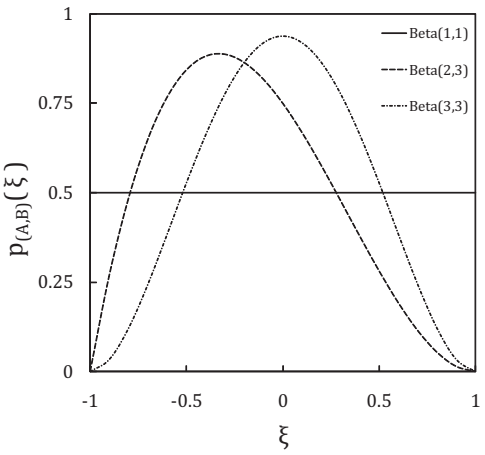


**Figure 4. Examples of beta PDF shapes for different combinations of $A$ and $B$**

### III.B. Stochastic Collocation

Once the sources of uncertainty have been identified and quantified by appropriate probability distributions, the effects of uncertainty can be studied using two methods: intrusive[18,23–25] and non-intrusive.[16,19,26] Hypersonic aerothermoelastic problems require the use of non-intrusive methods due to the complexity of comprehensive analysis codes.

Direct Monte Carlo simulation is the most widely used non-intrusive approach in relatively simple aeroelasticity studies.[16,17,27–33] This method requires numerous evaluations of the function of interest (e.g. flutter Mach number), at values of the uncertain inputs dictated by their probability distributions. The computational cost associated with numerous analysis evaluations is prohibitive for complex problems such as hypersonic aeroelastic and aerothermoelastic analysis. Therefore, SC is employed in this study as a computationally efficient alternative to direct MCS.

In SC, computationally efficient polynomial response surfaces are used to approximate the functional relationship between uncertain inputs $\xi$, and the output of interest $f(\xi)$, where $\xi$ is a normalized random variable varying between the limits -1 and 1.

$$f(\xi) \approx \hat{f}(\xi) = \sum_{j=1}^{P+1} A_j \phi_j(\xi) \tag{3}$$

The response surface $\hat{f}$ given by Eq. 3 consists of an expansion in terms of polynomial basis functions $(\phi_j(\xi))_{1<j<P+1}$, in which $A_j$'s are fitting coefficients, and $P+1$ represents the number of basis functions. Once constructed, MCS can be applied to the computationally inexpensive polynomial response surface in order to obtain the probability distribution associated with the output of interest.

In the current study, the expensive analyses are evaluated at a set of inputs $\xi$, called collocation points. The collocation points are chosen such that mean $m_f$, given by Eq. 4, and variance ${\sigma_f}^2$, given by Eq. 5, are numerically estimated using a numerical integration scheme defined by $N_I$ integration points, $(\xi_k)_{k=1,N_I}$ and their corresponding weights $(w_k)_{k=1,N_I}$. Thus the collocation points correspond to the numerical integration points.

$$m_f \equiv \langle f \rangle = \int_{\Omega} p\left(\xi\right) f\left(\xi\right) d\xi \simeq \sum_{k=1}^{N_I} w_k f(\xi_k) \tag{4}$$

$${\sigma_f}^2 \equiv \left\langle \left(f - \langle f \rangle\right)^2 \right\rangle = \int_{\Omega} p\left(\xi\right) \left(f\left(\xi\right) - \langle f \rangle\right)^2 d\xi \simeq \sum_{k=1}^{N_I} w_k \left(f\left(\xi_k\right) - \langle f \rangle\right)^2 \tag{5}$$

For the one dimensional case, the polynomial response surface, given by Eq. 3, is generated using Lagrange polynomials $(\phi_j)_{j=1,P+1}$, Eq. 6 associated with the collocations points $(\xi_k)_{k=1,N_I}$, Eq. 7.

$$\phi_j(\xi) = \prod_{k=1,k\neq j}^{N_I} \frac{\xi - \xi_k}{\xi_j - \xi_k} \quad j = 1, P+1 \tag{6}$$

$$\phi_j(\xi_k) = \delta_{jk} \quad k = 1, N_I \quad j = 1, P+1 \tag{7}$$

The degree of the polynomial approximation $P$, in Eqs. 6 and 7 is equal to $N_I - 1$.

For a multidimensional random input space, $\boldsymbol{\xi} = (\xi^{i_v})_{i_v=1,N_v}$, in which $N_v$ is the number of uncertain inputs, the multi-variate extension of Eq. 6 is given by Eq. 8.

$$\phi_j(\boldsymbol{\xi}) = \prod_{i_v=1}^{N_v} \prod_{k=1,k\neq j}^{N_I} \frac{\xi^{i_v} - \xi_k^{i_v}}{\xi_j^{i_v} - \xi_k^{i_v}} \quad j = 1, P+1 \tag{8}$$

For beta distributions, the corresponding numerical integration scheme is computed using Gaussian quadrature developed by Golub.[34] For a single random variable, the numerical integrations points are the roots of the Legendre polynomial function of degree $N_I$ associated with the beta probability distribution of the input. The numerical integration scheme is exact for polynomial functions of order less than $2N_I - 1$. In the two-dimensional case, the collocation points are depicted in Fig. 5 for beta distributions corresponding to various combinations of $A$ and $B$ for $N_I = 7^2$. This method tends to concentrate collocation points in the regions of higher probability. For instance integration points associated with the Beta(3,3) PDF have a higher concentration at the center of the domain compared to the grid associated with Beta(1,1).

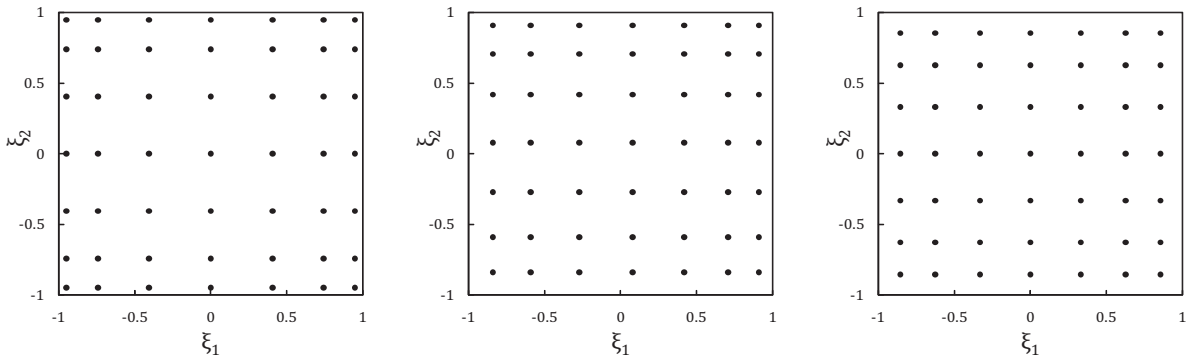


(a) Beta(1,1) (b) Beta(3,2) (c) Beta(3,3)

**Figure 5. Collocation points for 2 random variable for different beta distributions, $N_I = 7^2$**

Since there is strong evidence that SC approach has outperformed polynomial chaos expansion,[19] another widely used technique, SC is the method chosen for this study. It should be noted however that this method suffers from the curse of dimensionality which implies that increasing the number of random inputs exponentially increases the number of analysis runs and the computational cost of the method. The number of analyses required for the implementation of the SC approach is $(P+1)^{N_v}$. Furthermore the collocation points associated with most integration schemes are located strictly within the domain of the input variable. Therefore, extrapolation is required for response surface evaluations close to the domain boundaries which may adversely affect accuracy. Other efficient interpolation techniques can be considered to create the response surface such as adaptive sparse grid interpolation,[35,36] Kriging surrogates[37] or multi-variable splines[38,39] if discontinuities are present. The investigation of such approaches is the subject of ongoing research beyond the scope of this paper.

## IV. Results

This section presents uncertainty propagation results applied to both case studies described in Section II. The importance of non-deterministic approaches for hypersonic vehicle analysis is characterized by comparing

with results obtained from deterministic analyses. In all results, the 95 % confidence interval for the flutter Mach number and minimum and maximum values are obtained by conducting $10^5$ Monte Carlo simulations on the approximate problem, i.e. the polynomial response surface, using the **MATLAB** random number generator *betarnd*.

### IV.A. Uncertainty Propagation for 2D typical Section

The system is characterized by the parameters given in Table 1, which were taken from Ref. 2. Variability is introduced in the natural uncoupled frequencies in order to represent uncertainty related to stiffness and/or mass properties in a more complex system. The range for each uncertain input is taken to be ±50% of their baseline value, and the respective probability distribution is chosen to be uniform – see Table. 2.

**Table 1. Baseline configuration for the typical section**

| Parameter | | Value | Units |
|---|---|---|---|
| Altitude | $H$ | [0 100,000] | ft |
| Elastic axis location | $a$ | [-0.4 0.4] | N/A |
| Chord | $c$ | 2.35 | m |
| Thickness | $\tau$ | 3.36 | % |
| Center of gravity location | $x_\alpha$ | 0.2 | N/A |
| Bending frequency | $\omega_h$ | 13.4 | Hz |
| Torsional frequency | $\omega_\alpha$ | 37.6 | Hz |

**Table 2. Uncertain parameters associated with the 2D typical section**

| Parameter | Baseline value | Range | Distribution |
|---|---|---|---|
| Bending frequency | 13.4 Hz | [-50% +50%] | Uniform |
| Torsional frequency | 37.6 Hz | [-50% +50%] | Uniform |

Selection of the degree required for the SC expansion, was based on a convergence study. In the convergence study, $a$ and $H$ were fixed at 0.0 and 40,000 feet respectively. The mean and the variance associated with the flutter Mach number obtained from polynomial expansion up to $10^{th}$ order were compared to results obtained from a $15^{th}$ order expansion based on $(15+1)^2 = 256$ analysis evaluations. The relative errors associated with the mean and standard deviation are shown in Fig. 6(a). Furthermore, the accuracy of the various polynomial expansions was quantified by comparing the response surface predictions with the values obtained from the 256 evaluations associated with the reference case. For this 256-points set, maximum and sum of squares (L2) relative errors between the computed value and the response surface prediction was computed and are shown in Fig. 6(b). The maximum error is less than 1% for a response surface based on a $6^{th}$ order expansion (i.e. 49 collocation points). Based on these results the corresponding $6^{th}$ order polynomial expansions were used in additional investigations corresponding to various values for the elastic axis offset $a$ and the altitude $H$.

Uncertainties associated with the pitch and plunge natural frequencies are propagated to the flutter Mach number using a $6^{th}$ order polynomial response surface generated by stochastic collocation for an elastic axis offset, $a$, varying from -0.4 to 0.4 at an altitude of 40,000 feet. In Fig. 7, the deterministic flutter Mach number is compared to the mean, and standard deviation in flutter Mach numbers due to the uncertainties. The results show that the mean of the flutter Mach number is close to the deterministic value. The standard deviation varies from 36% to 53% of the deterministic value, as indicated by the shaded boxes in Fig. 7. Furthermore, an interval likely to include the flutter Mach number with 95% confidence is depicted using error bars in Fig. 7. This interval varies from as low as -79%, to as high as +94% of the deterministic value. These results are also concisely summarized in Table. 3. The corresponding output probability distributions are illustrated by Fig. 8 for different elastic axis offsets $a$. It is clear from Fig. 8 that there is

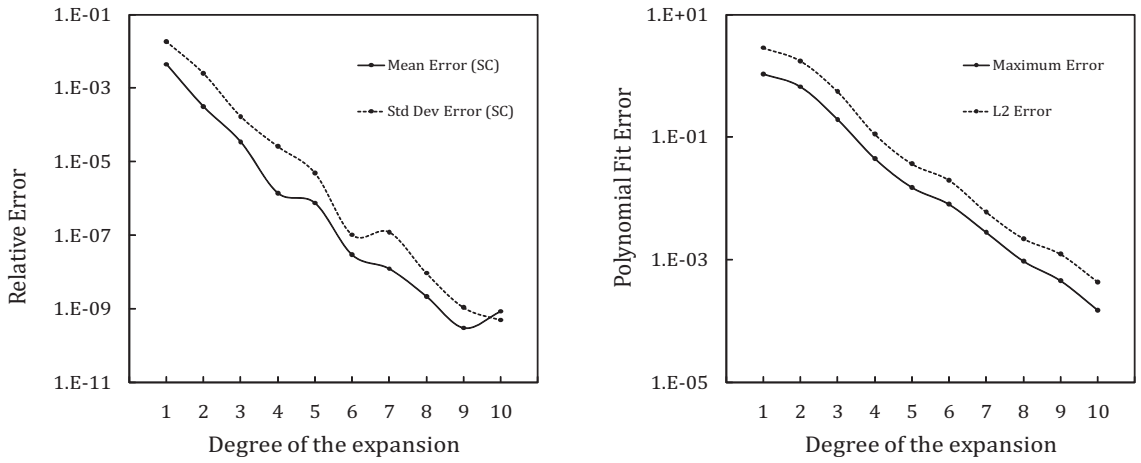


(a) Mean and variance prediction error

(b) Approximation error

**Figure 6. Convergence study for SC method, $a = 0$, $H = 40{,}000$ ft**

a significant probability that the system will flutter before its deterministically predicted value. Therefore, non–deterministic approaches are required to properly quantify the aeroelastic stability boundary.

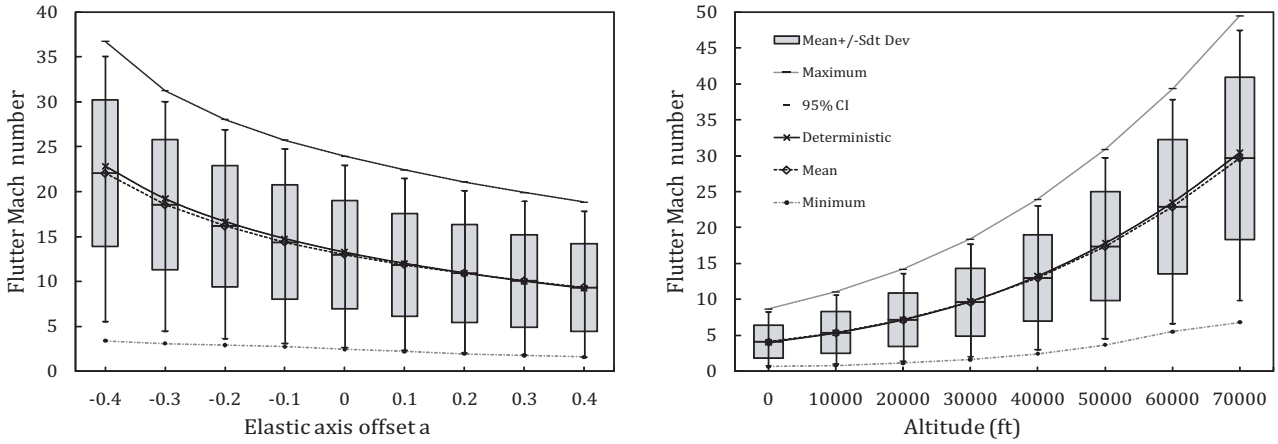


(a) $H = 40{,}000$ ft

(b) $a = 0$

**Figure 7. Uncertainty propagation results for varying elastic axis (a) or altitude (b)**

Additional information can be extracted from the probabilistic nature of the uncertainty quantification analysis, as illustrated in Fig. 9, which shows the probability that the flutter Mach number will be less than some percentage of the deterministic prediction. For example, depending on the value of the elastic offset, there is a 12–23% probability that the control surface will flutter at a Mach number that is 50% less than the deterministic prediction, when assuming a PDF corresponding to Beta(1,1).

These results demonstrate that uncertain inputs can produce significant levels of uncertainty in predicted flutter Mach numbers. By treating the problem in a probabilistic manner, more information about the prediction is extracted. In this particular case the deterministic analysis is not sufficient since large variations in the flutter Mach number due to the assumed uncertainties were observed.

The effect of the input probability distribution shape of the random inputs on the stochastic output probability distribution is also studied. The same framework was followed for different input probability distributions. The range for the frequencies is unchanged. Both $\xi_1$ and $\xi_2$ have the same probability distribution for all cases shown in Figs. 9 and 10. The results display a significant effect of the probability

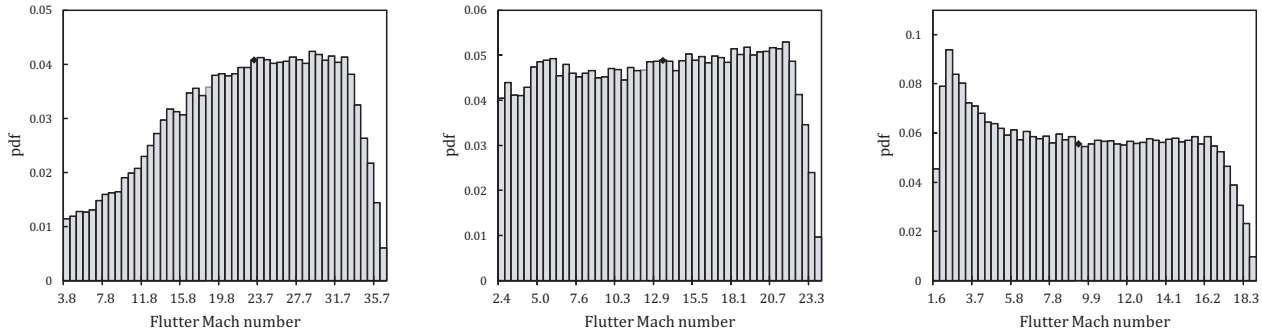


(a) $a = -0.4$ (b) $a = 0$ (c) $a = 0.4$

**Figure 8. Flutter Mach number PDF prediction using a 6th order polynomial expansion in SC, $H$ = 40,000 ft, *the black dot indicates the deterministic value***

**Table 3. Flutter Mach number variability, $H$ = 40,000 ft**

| Elastic offset | $a = -0.4$ | $a = 0$ | $a = 0.4$ |
|---|---|---|---|
| Deterministic value | 22.8 | 13.3 | 9.2 |
| Mean | 22.1 *(-3.4%)* | 13 *(-1.9%)* | 9.3 *(+ 0.9%)* |
| Standard deviation | 8.2 *(35.8%)* | 6 *(45.5%)* | 4.9 *( 53.2%)* |
| 95% confidence interval | 5.9 - 34.9 | 3 - 23 | 2 - 17.9 |
| | *-74.3%, +53.3%* | *-77.1%, +73.8%* | *-78.7%, +94.2%* |
| Range | 3.4 - 36.7 | 2.4 - 23.9 | 1.6 - 18.8 |
| | *-85.1%, +60.9%* | *-91.6%, +80.6%* | *-82.9%, +104.1%* |

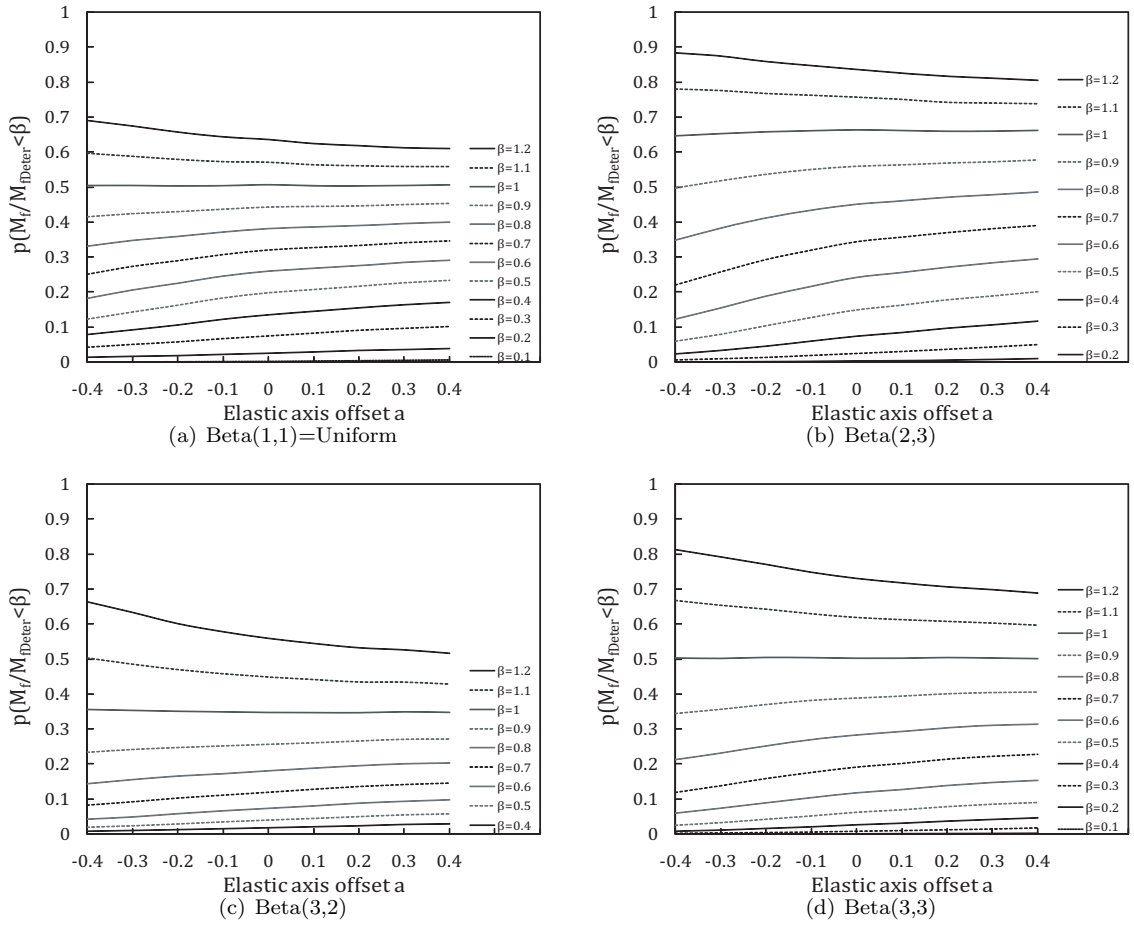


(a) Beta(1,1)=Uniform (b) Beta(2,3)

(c) Beta(3,2) (d) Beta(3,3)

**Figure 9.** $p(\frac{M_f}{M_{f,deter}} < \beta)$ **for different inputs probability distributions ,** $H$ **= 40,000 ft**

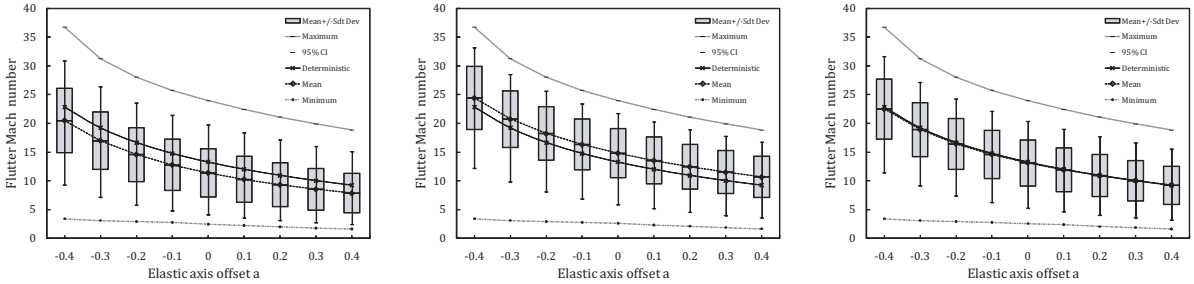


(a) Beta(2,3) (b) Beta(3,2) (c) Beta(3,3)

**Figure 10. Uncertainty propagation results for different input probability distribution,** $H$ **= 40,000 ft**

distribution of the input as shown by Figs. 9(b), (c) and (d) and Fig. 10. The choice of input probability distribution affects all the stochastic analysis quantities i.e. mean or expected value, standard deviation and 95% confidence interval. As expected maximum and minimum remain unchanged since the ranges of the uncertain inputs were not changed.

When considering these results, it is important to note that the altitude ($H$ = 40,000 ft) at which the aeroelastic studies are conducted is not representative of hypersonic flight. However more realistic altitudes of 80,000-100,000 ft produce very high Mach numbers, and therefore the altitude was artificially reduced in order to reduce these to practical values. However, as pointed out in Ref. 40, incorporation of aerodynamic heating leads to a reduction of the flutter Mach number, and thus aerothermoelastic studies can be conducted at more reasonable altitudes.

### IV.B. Uncertainty Propagation for Aerothermoelastic Problem of a Panel

This problem, described in Section II.B, is defined by the parameters provided in Table 4. The altitude considered is 98,500 feet and the freestream Mach number varies from 8 to 12. The forebody inclination is 5 degrees, the panel is assumed to be 1.5 meters long and is located at a distance of 1.0 meter from the leading edge of the panel. The flow over the panel is assumed to be fully turbulent which implies that the transition region is arbitrarily assumed to start at the leading edge of the vehicle and to end before the leading edge of the panel. Consequently in this problem, uncertainty is introduced in the heat flux transfer computations.

**Table 4. Baseline configuration for the panel**

| Parameter | | Value | unit |
|---|---|---|---|
| Altitude | $H$ | 98,500 | ft |
| Freestream Mach number | $M$ | 8-12 | N/A |
| Forebody surface inclination | $\theta$ | 5 | deg |
| Panel Length | $l_p$ | 1.5 | m |
| Panel Thickness | $h_p$ | 5 | mm |
| Initial panel temperature | $T_0$ | 300 | K |
| Distance of leading edge of the panel from leading edge of the vehicle | $x_e$ | 1.0 | m |
| Transition to turbulence upstream of panel | $x_{ti}$ | 1.0 | m |

Appropriate modeling of turbulence and gas properties is a key factor for accurate prediction of the aerodynamic heat flux on the structure. In Ref. 13, two sources of uncertainty have been identified. The first is associated with uncertainty in turbulence modeling, and the second pertains to uncertainty in the transition from laminar to turbulent flow. Both affect the heat flux, and thus have a direct impact on the aerothermoelastic stability of the panel.

Turbulence Modeling The uncertainty due to turbulence modeling was quantified by comparing Eckert's reference enthalpy model[21] with full order CFD results based on two turbulence models; this comparison is depicted in Fig. 11. The full order results were generated with the CFL3D CFD solver. The flight Mach number is 8.0, and the temperature on the panel surface is 900 Kelvin. For the given panel deflections shown in Figs. 11(a) and (c), the predicted heat flux distributions along the panel computed from the various models are illustrated in Figs. 11(b) and (d). Depending on the model used to compute the convective heat flux, the results differ. Four different predictions are compared: two based on CFD computations with different turbulence models, and two based on Eckert's reference enthalpy and reference temperature models. The models considered in Fig. 11 result in similar spatial distribution shapes for the heat flux and differ only in offsets of the heat flux.

Based on these observations, uncertainty due to turbulence modeling is characterized as follows: the variation in heat flux predictions based on the differences between Eckert's reference enthalpy model and the two CFD codes with different turbulence models, is accounted for by using a scaling factor $\alpha_q$ that modifies the Eckert's reference enthalpy heat flux to yield $\alpha_q Q_{aero}$. The range in $\alpha_q$ was chosen to be $0.95 < \alpha_q < 1.25$ in order to encompass the difference between Eckert's reference enthalpy and the two CFD turbulence models

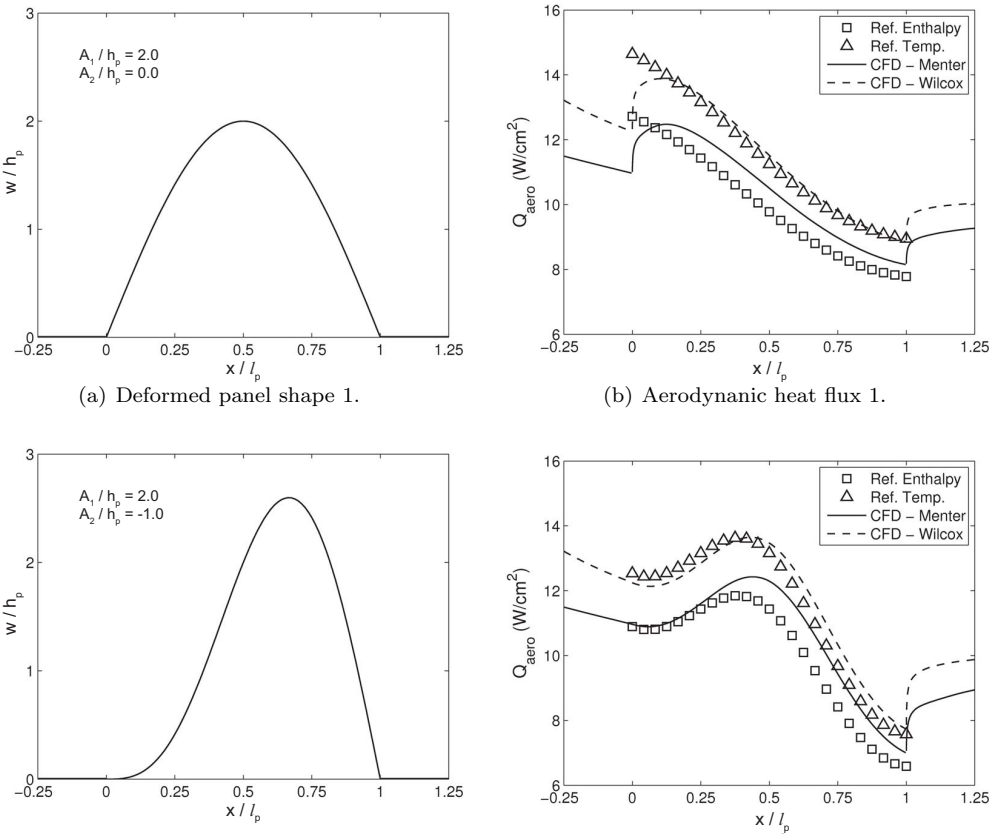


(a) Deformed panel shape 1.

(b) Aerodynamic heat flux 1.

(c) Deformed panel shape 2.

(d) Aerodynamic heat flux 2.

**Figure 11. Comparison of aerodynamic heating predictions over two deformed panel shapes, $T_{wall} = 900K$, $M = 8$, from Refs. 13, 14**

depicted in Fig. 11 (b) and (d). A value of $\alpha_q = 1$ corresponds to the baseline value employed in Ref. 14. The probability distribution for $\alpha_q$ was assumed to be uniform, i.e. $Beta(1, 1)$.

Transition Location Prediction In addition to the uncertainty associated with the turbulence model, the uncertainty associated with the location of the onset of turbulence was also modeled. In Ref. 13, the location at which the flow transition from laminar to turbulent was arbitrarily chosen to correspond to the distance between the leading edge of the vehicle and the leading edge of the panel. Transition modeling in hypersonic flow is a very complex issue. The location of the transition region depends on numerous parameters such as flight conditions, wall temperature, surface roughness or preexisting disturbances level in the flow.[7]

Transition uncertainty quantification was aided by use of the CFD++ commercial CFD solver. The CFD++ code is a powerful computational fluid dynamic code which contains several turbulence models. A recommended turbulence model for external hypersonic aerodynamic predictions is the $k - \epsilon$ model. To model the transition location, an algebraic transition (AT) model is used in conjunction with the $k - \epsilon$ model.[41] It triggers transition based on detection of local flow curvature by augmenting local shear stress.

For each of the additional turbulence equations, boundary conditions are needed. The dependant variable associated with each freestream boundary condition can be computed given two freestream turbulence characteristic parameters: the turbulent kinetic energy intensity, $T_u$ (which varies from 0.1 to 1% for external flows according to 'CFD++ Best Practices'[41]) and the turbulent to laminar viscosity ratio, $\mu_T/\mu$, (which varies from 2 to 5). The combination of both parameters characterizes the level of turbulence in the freestream flow. However, these parameters are rarely known[41] and therefore should be treated as uncertain parameters. To estimate their impact on the heat flux prediction, or more precisely on laminar to turbulent transition region location on the vehicle, four simulations were computed for different cases which correspond

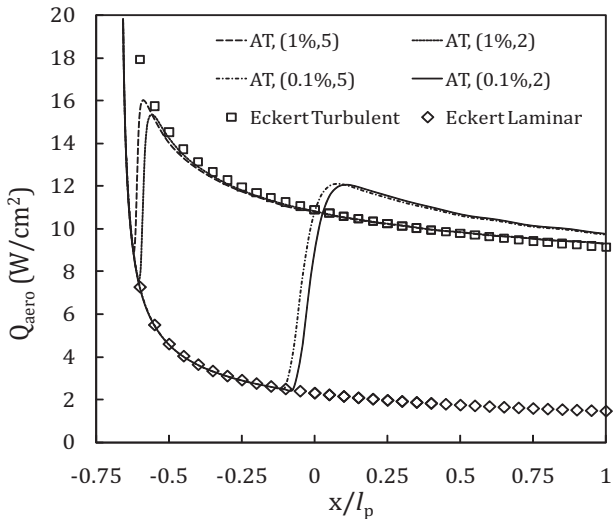


**Figure 12. Heat flux prediction using CFD++ $k-\epsilon$ augmented with algebraic transition model (AT),** $T_{wall} = 900K$, $M = 8$

to the extreme values of both parameters. For level flight at Mach 8 and a constant wall temperature of 900 K, the location of the turbulence transition region can be ascertained from the heat flux distributions shown in Fig. 12. The sharp vertical increases in heat flux indicate transition from laminar to turbulent flow. Turbulence transition location for different values of kinetic energy intensity varies from close to the leading edge of the vehicle, which corresponds to $x/l_p = -0.67$, up to the leading edge of the panel ($x/l_p = 0$).

In the deterministic analysis it was assumed that the panel was under fully developed turbulent flow. This assumption is a very conservative one. For laminar flows the aerodynamics heat flux on the panel is of the order of one fifth of the heat flux due to turbulent flows. However, even for this assumption, there is uncertainty associated with the location of the transition due to variability in the turbulence level of the freestream flows. In order to quantify the effects of uncertainty associated with the turbulence onset location, $x_{ti}$, the distance of the onset location from the leading edge of the panel was varied from 0.2 meter to 1 meter corresponding to $-0.67 \leq x_{ti}/l_p \leq -0.1$. The distance of 1 meter corresponds to an onset of turbulent flow at the leading edge of the vehicle, which represents the baseline value assumed in Ref. 13. The turbulence onset location is assumed to be uniformly distributed between 0.2 meter and 1 meter.

**Table 5. Uncertain Parameters**

| Parameter | Baseline value | Range | Distribution |
|---|---|---|---|
| $\alpha_q$ | 1 | [0.95 1.25] | Uniform |
| Transition region start | -1 m | [-1 -0.2] (m) | Uniform |

Both uncertainties associated with the turbulence model and the transition location, summarized in Table 5, were propagated through the analysis and their impact on the flight time was determined. A $6^{th}$ order polynomial response surface was constructed based on 49 analysis runs; i.e. 7 collocation points for the two random variables. Uncertainty propagation results for different Mach numbers are shown Fig. 13(a). In Fig. 13(b) results are normalized with respect to the deterministic value. At Mach 8 the mean value of the flight time was 922 sec, compared to the deterministic value of 1003 sec. The standard deviation and range are 4.51 sec (4%) and 820–1003 sec ([-16%, +2.4%]) respectively, where percentages are in terms of the deterministic value. Furthermore, the output probability distribution, shown in Fig. 14, indicates a significant probability that the flight time will be much less than its deterministic value. These results clearly demonstrate the importance of incorporating uncertainty in a more complicated aerothermoelastic problem.

The same uncertainty was propagated at different Mach numbers, and a concise summary of the probability results is given in Table 6. The computed probability distributions for additional Mach numbers are given in Fig. 15. The ranges for $\alpha_q$ and the transition location determined from Mach 8 results were used

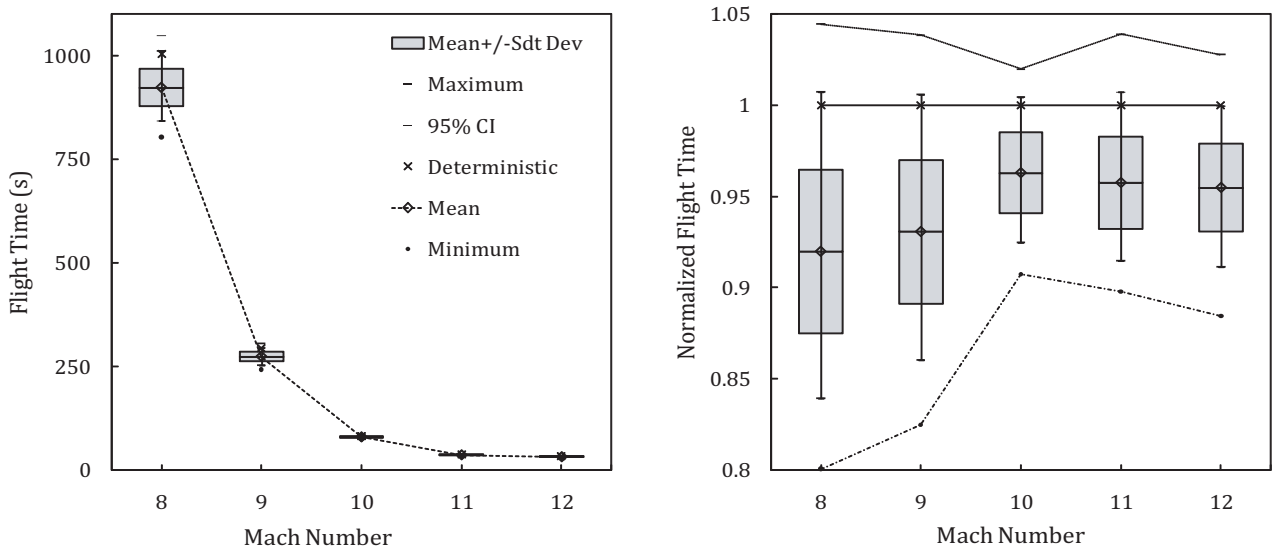


(a) Flight time

(b) Normalized flight time

**Figure 13. Flight time as a function of flight Mach number**

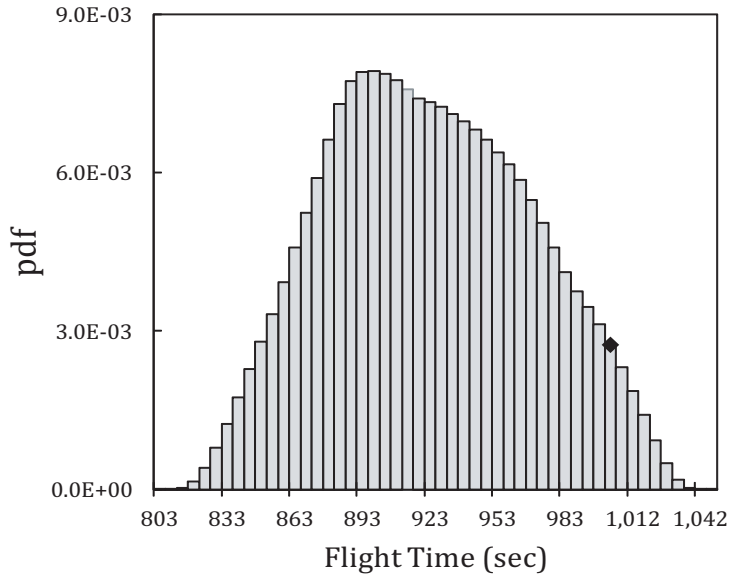


**Figure 14. PDF for the flight time at Mach 8, $H$ = 98,500 ft** ***(the black dot indicates the deterministic value)***

**Table 6. Flight Time variabilty**

| Mach Number | $M = 8$ | $M = 9$ | $M = 10$ |
|---|---|---|---|
| Deterministic value (sec) | 1002.8 | 294.3 | 82.8 |
| Mean (sec) | 922.4 *(-8.0%)* | 273.9 *(-6.9%)* | 79.7 *(+ 0.9%)* |
| Standard deviation (sec) | 45.1 *(4.5%)* | 11.6 *(3.9%)* | 1.8 *( 53.2%)* |
| 95% confidence interval (sec) | 841.8 - 1009.9 | 253.2 - 296.1 | 76.6 - 83.1 |
| | *-16.1% , +0.7%* | *-14.0%, +73.8%* | *-7.5%, +0.4%* |
| Range (sec) | 819.9 - 1029.2 | 247.3 - 300.9 | 75.2 - 83.8 |
| | *-18.2%, +2.6%* | *-16.0%, +2.2%* | *-9.1%, +1.3%* |

in these computations. The inconsistent shapes shown in Figs. 15 (c) and (d) illustrate the limitations in the approach. Discrepancies are observed for Mach number 11 and 12. Approximately ±1 second errors in the estimations of flight time occur due to the method described in Section II.B. For lower Mach numbers, this error is insignificant compared to the stochastic variability of the output. However, for higher Mach numbers, this error becomes significant compared to the estimated flight times and significatively affects the response surface fit accuracy.

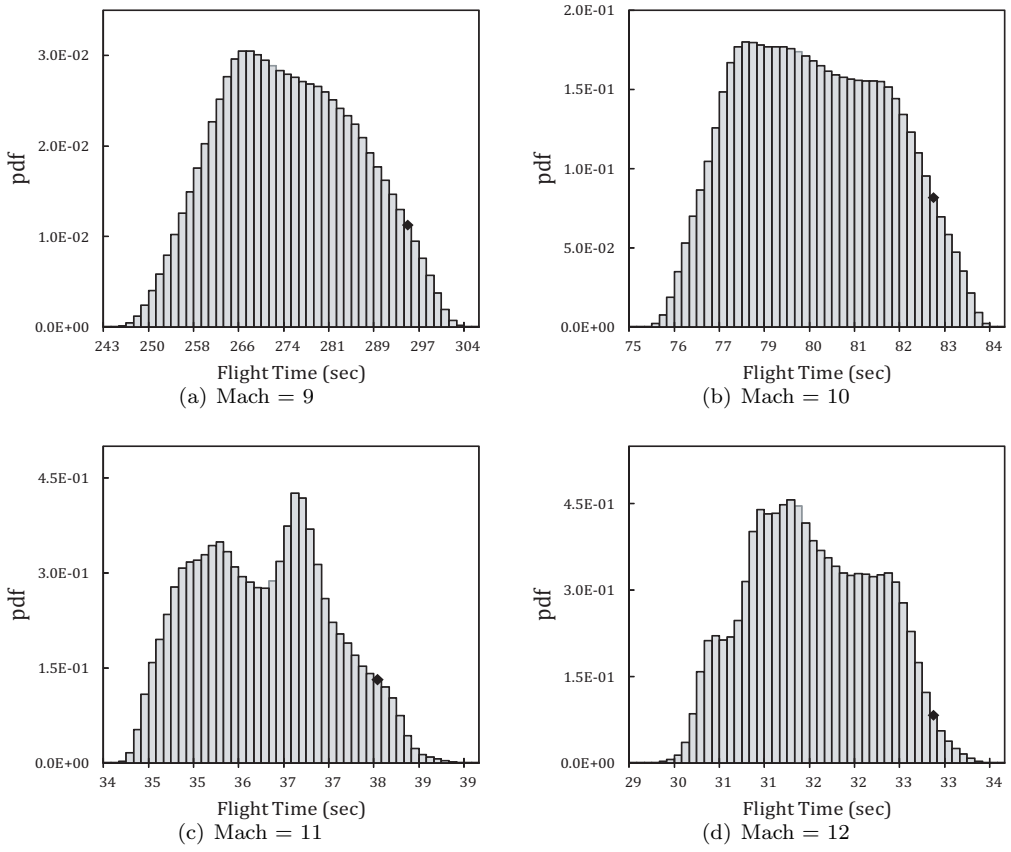


**Figure 15. PDF of the Flight time for 9 to 12 flight Mach number** *(the black dot indicates the deterministic value)*

## V. Concluding Remarks

Stochastic collocation is an efficient approach for propagating uncertainty in aeroelastic and aerothermoelastic analyses. Reduced order models used in hypersonic aeroelastic and aerothermoelastic analyses based on insufficient knowledge of pertinent physics associated with this class of problems require an uncertainty quantification approach. The results demonstrate that deterministic quantification of aeroelastic and aerothermoelastic stability boundaries is insufficient for hypersonic vehicle analysis and non deterministic approaches must be employed.

1. The aeroelastic stability of a typical section provides an illustrative example of the type of additional information that can be extracted using a probabilistic approach. The framework for uncertainty propagation for a hypersonic aeroelasticity example is presented in detail. Importance of the probability distribution of the random input is illustrated by the results that display a significant variation in flutter Mach number.

2. The aerothermoelastic stability of a panel represents a richer problem where uncertainty inherent with turbulence modeling and transition prediction introduce additional sources of error. Uncertainty in turbulence modeling and transition location have been identified and quantified using computational tools such as CFL3D and CFD++, two powerful CFD codes. Transition prediction is an ongoing area of research. Treating it as an uncertain parameter is necessary, and provides additional information about the reliability of the analysis. For this problem, despite the conservative hypothesis that the panel experiences fully developed turbulent flows, uncertainty associated with the transition location ahead of the panel influences the flight time predictions for the onset of instability.

## Acknowledgments

This research is funded under NASA grant NNX08AB32A with Donald Soloway and Jorge Bardina as technical monitors.

## References

[1]McNamara, J. J. and Friedmann, P. P., "Aeroelastic and Aerothermoelastic Analysis of Hypersonic Vehicles: Current Status and Future Trends," *Proceeding for the 48th AIAA/ASME/ASCE/AHS/ASC Structures, Structural Dynamics, and Materials Conference*, Honolulu, Hawaii, April 2007, AIAA Paper No. 2007-2013.

[2]McNamara, J. J., *Aeroelastic and Aerothermoelastic Behavior of Two and Three Dimensional Lifting Surfaces in Hypersonic Flow*, Ph.D. thesis, The University of Michigan, Ann Arbor, Michigan, 2005.

[3]Fidan, B., Mirmirani, M., and Ioannou, P. A., "Flight Dynamics and Control of Air-Breathing Hypersonic Vehicles: Review and New Directions," *Proceedings of the 12th AIAA International Space Planes and Hypersonic Systems and Technologies*, Norfolk, Virginia, December 15–19 2003, AIAA Paper No. 2003-7081.

[4]Hallion, R. P., "The History of Hypersonics: or, "Back to the Future - Again and Again"," *Proceedings of the 43rd Aerospace Sciences Meeting and Exhibit*, Reno,Nevada, January 10–13 2005, AIAA Paper No. 2005-329.

[5]Rodriguez, A. A., Dickeson, J. J., Cifdaloz, O., Kelkar, A., Vogel, J. M., and Soloway, D., "Modeling and Control of Scramjet-Powered Hypersonic Vehicles: Challenges, Trends, and Tradeoffs," *Proceedings of AIAA Guidance, Navigation and Control Conference and Exhibit*, Honolulu, Hawaii, August 18–21 2008, AIAA Paper No. 2008-6793.

[6]Dolvin, D. J., "Hypersonic International Flight Research and Experimentation (HIFiRE), Fundamental Sciences and Technology Development Strategy," *Proceedings of the 15th AIAA International Space Planes and Hypersonic System and Technologies Conference*, Dayton, Ohio, April 28 – May 1 2008, AIAA Paper No. -.

[7]Bertin, J. J., *Hypersonic Aerothermodynamics*, AIAA Education Series, 1938.

[8]Anderson, J. D., *Modern Compressible Flow with Historical Perspective*, Third Edition Mc Graw Hill Editions, 2004.

[9]Dugundji, J. and Calligeros, J. M., "Similarity Laws for Aerothermoelastic Testing," *Journal of Aerospace Sciences*, Vol. 29, No. 8, Aug. 1962, pp. 935–950.

[10]Olejniczak, J., Candler, G. V., Wright, M. J., Hornung, H. G., and Leyva, I., "High Enthalpy Double-Wedge Experiments," *Proceedings of the 19th AIAA, Advanced Measurement and Ground Testing Technology Conference*, New Orleans, LA, June 17–20 1996, AIAA Paper No. 96-2238.

[11]Smith, V. K., Laster, M. L., and Boudreau, A. H., "Test and Evaluation Challenges for Hypersonic Air-Breathing Propulsion Systems," 1994, AIAA Paper No. 94-2675-CP.

[12]Cox, C., Lewis, C., Pap, R., Golver, C., Priddy, K., Edwards, J., and McCarty, D., "Prediction of Unstart Phenomena in Hypersonic Aircraft," *Proceedings of the AIAA 6th International Aerospace Planes and Hypersonics Technologies Conference*, Chattanooga, TN, April 3–7 1995, AIAA Paper No. 95-6018.

[13]Culler, A. J., Crowell, A. R., and McNamara, J. J., "Studies on Fluid-Structural Coupling for Aerothermoelasticity in Hypersonic Flow," *Proceedings of the 50th AIAA/ASME/ASCE/AHS/ASC Structures, Structural Dynamics, and Materials Conference*, Palm Springs, CA, May 4–7 2009, AIAA Paper No. 2009-2364.

[14]Crowell, A. R., Culler, A. J., and McNamara, J. J., "Reduced Order Aerothermodynamics for Two-Way Coupled Aerothermoelasticity in Hypersonic Flow," *International Forum for Aeroelasticity and Structural Dynamics 2009*, Seattle, WA, June 21-25 2009, IFASD-2009-094.

[15]Falkiewicz, N. J. and Cesnik, C. E. S., "A Reduced-Order Modeling Framework for Integrated Thermo-Elastic Analysis of Hypersonic Vehicles," *Proceedings of the 50th AIAA/ASME/ASCE/AHS/ASC Structures, Structural Dynamics and Materials Conference*, Palm Springs, California, May 4–7 2009, AIAA Paper No. 2009-2308.

[16]Murugan, S., Harursampath, H., and Ganguli, R., "Material Uncertainty Propagation in Helicopter Nonlinear Aeroelastic Response and Vibration Analysis," *AIAA Journal*, Vol. 46, No. 9, Sept. 2008, pp. 2332–2344.

[17]Beran, P. S. and Pettit, C. L., "A Direct Method for Quantifying Limit Cycle Oscillations Response Characteristics in the Presence of Uncertainties," *Proceedings of the 45th AIAA/ASME/ASCE/AHS/ASC Structures, Structural Dynamics, and Materials Conference*, Palm Springs, CA, April 19-22 2004, AIAA Paper No. 2004-1695.

[18]Witteveen, J. A. S., Loeven, A., and Bijl, H., "An adaptive Stochastic Finite Elements approach based on Newton Cotes Quadrature in Simplex Elements," *Computers and Fluids Journal*, Vol. 38, 2009, pp. 1270–1288.

[19]Eldred, M. S. and Burkardt, J., "Comparison of Non-Intrusive Polynomials Chaos and Stochastic Collocation Methods for Uncertainty Quantification," *Proceedings of the 47th AIAA Aerospace Sciences Meeting Including The New Horizons Forum and Aerospace Exposition*, Orlando, Florida, January 5–8 2009, AIAA Paper No. 2009-976.

[20]McNamara, J. J. and Friedmann, P. P., "Flutter Boundary Identification for Time-Domain Computational Aeroelasticity," *AIAA Journal*, Vol. 45, No. 7, July 2007, pp. 1546–1555.

[21]Eckert, E. R. G., "Engineering Relations for Heat Transfer and Friction in High-Velocity Laminar and Turbulent Boundary Layer Over Surfaces With Constant Pressure and Temperature," *Transactions of the ASME*, Vol. 78, No. 6, June 1956, pp. 1273–1283.

[22]Haldar, A. and Mahadevan, S., *Probability, Reliability and Statistical Methods in Engineering Design*, Jon Wiley and Sons, Inc., 2000.

[23]Ghanem, R. G. and Spanos, P. D., *Stochastic Finite Elements, a Spectral Approach, Revised Edition*, Dover, 1991.

[24]Mathelin, L., Hussaini, M. Y., and Zang, T. A., "Stochastic Approaches to Uncertainty Quantification in CFD Simulations," *Numerical Algorithms Journal*, Vol. 38, No. 1, March 2005, pp. 209–236.

[25]Walters, R. W., "Towards Stochastic Fluid Mechanics via Polynomial Chaos," *Proceedings of the 41st Aerospace Sciences Meeting and Exhibit*, Reno, Nevada, January 6–9 2003, AIAA Paper No. 2003-413.

[26]Eldred, M. S., Webster, C. G., and Constantine, P. G., "Design Under Uncertainty Employing Stochastic Expansion Methods," *Proceedings of the 12th AIAA/ISSMO Multidisciplinary Analysis and Optimization Conference*, Orlando, Florida, September 10–12 2008, AIAA Paper No. 2008-6001.

[27]Pettit, C., "Uncertainty Quantification in Aeroelasticity: Recent Results and Research Challenges," *Journal of Aircraft*, Vol. 41, No. 5, September-October 2008, pp. 1217–1229.

[28]Hosder, S., Walters, R. W., and Balch, M., "Efficient Uncertainty Quantification Applied to the Aeroelastic Analysis of a Transonic Wing," *Proceedings of the 46th AIAA Aerospace Sciences Meeting and Exhibit*, Reno, Nevada, January 7-10 2008, AIAA Paper No. 2008-729.

[29]Styuart, A. V., Mor, M., Livne, E., and Lin, K. Y., "Aeroelastic Failure Risk Assessment in Damage Tolerant Composite Airframe Structures," *Proceedings of the 48th AIAA/ASME/ASCE/AHS/ASC Structures, Structural Dynamics, and Materials Conference*, Honolulu, Hawaii, April 23-26 2007, AIAA Paper No. 2007-1981.

[30]Lindsley, N. J., Beran, P. S., and Pettit, C. L., "Integration of Model Reduction and Probabilistic Techniques with Deterministic Multi-physics Models," *Proceedings of the 44th AIAA Aerospace Sciences Meeting and Exhibit*, Reno, Nevada, January 9-12 2006, AIAA Paper No. 2006-192.

[31]Lindsley, N. J., Beran, P. S., and Pettit, C. L., "Effects of Uncertainty on Nonlinear Plate Response in Supersonic Flow," *Proceedings of the 9th AIAA/ISSMO Symposium on Multidisciplinay Analysis and Optimization*, Atlanta, Georgia, September 4-6 2002, AIAA Paper No. 2002-5600.

[32]Kurdi, M., Lindsley, N., and Beran, P., "Uncertainty Quantification of the Goland Wing's Flutter Boundary," *Proceedings of the AIAA Atmospheric Flight Mechanics Conference and Exhibit*, Hilton Head, South Carolina, August 20-23 2007, AIAA Paper No. 2007-6309.

[33]Choi, S.-K., Grandhi, R. V., Canfield, R. A., and Pettit, C. L., "Polynomial Chaos Expansion with Latin Hypercube Sampling for Estimating Response Variability," *AIAA Journal*, Vol. 42, No. 6, June 2004, pp. 1191–1198.

[34]Golub, G. H. and Welsch, J. H., "Calculation of Gauss Quadrature Rules," Technical Report CS 81, School of Humanities and Sciences, Computer Sciences Department, Stanford University, November 3 1967.

[35]Klimke, A., *Sparse Grid Interpolation Toolbox User's Guide, v5.1*, Institute für Angewandte Analysis und Numerische Simulation (IANS), Universität Stuttgart, 2008, ISSN 1611-4176.

[36]Bunjgartz, H.-J. and Dirnstorfer, S., "Multivariate Quadrature on Sparse Grids," *Computing, Archives for Scientific Computing*, Vol. 71, No. 1, August 23 2003, pp. 84–114.

[37]Sacks, J., Welch, W. J., Mitchell, T. J., and Wynn, H. P., "Design and Analysis of Computer Experiments," *Statistical Science*, Vol. 4, No. 4, 1989, pp. 409–435.

[38]Jekabsons, G., *Adaptive Regression Splines toolbox for Matlab,ver. 1.3*, Institute of Applied Computer Systems, Riga Technical University, 2009, Reference manual.

[39]Friedman, J. H., "Multivariate Adaptive Regression Splines," *The Annals of Statistics*, Vol. 19, No. 1, March 1991, pp. 1–67.

[40]McNamara, J. J., Friedmann, P. P., Powell, K., Thuruthimattam, B., and Bartels, R., "Aeroelastic and Aerothermoelastic Behavior in Hypersonic Flow," *AIAA Journal*, Vol. 46, No. 10, Oct. 2008, pp. 2591–2610.

[41] Metacomp Technologies, Inc., *CFD++ User Manual - Version 8.1*, 2009.